JOURNAL OF SPACECRAFT AND ROCKETS
Vol. 31, No. 6, November–December 1994

Thermal Response and Ablation Characteristics of Lightweight Ceramic Ablators

Huy K. Tran* and Daniel J. Rasky†
NASA Ames Research Center, Moffett Field, California 94035-1000
and
Lili Esfahani‡
San Jose State University, San Jose, California 95129

This paper presents the thermal performance and ablation characteristics of the newly developed lightweight ceramic ablators (LCAs) in a supersonic, high-enthalpy convective environment. Lightweight ceramic ablators were recently conceived and developed at NASA Ames using low-density ceramic or carbon fibrous matrices as substrates for main structural support and organic resins as fillers. These LCAs were successfully produced with densities ranging from ≈0.224 to 1.282 g/cm^3. Several infiltrants with different char yields were used to study the effect on surface recession. Tests were conducted in the NASA Ames arc-jet facilities. Material thermal performance was evaluated at cold-wall heat fluxes from 113.5 to 1634 W/cm^2, and stagnation pressures of 0.018 to 0.331 atm. Conventional ablators such as SLA-561, Avcoat 5026-39HC, MA-25S, and balsa wood were tested at the same heat fluxes for direct comparison. Surface temperature was measured using optical pyrometers, and the recession rates were obtained from the high-speed films. In-depth temperature data were obtained to determine the thermal penetration depths and conductivity. Preliminary results indicated that most LCAs performed comparably to or better than conventional ablators. At low flux levels (<454 W/cm^2), the addition of silicon carbide and polymethyl methacrylate significantly improved the ablation performance of silica substrates. The carbon-based LCAs were the most mass-efficient at high flux levels (>454 W/cm^2).

Nomenclature

F	= radiation view factor
H	= effective heat of ablation, kJ/kg
h	= total enthalpy, J/kg
$\dot{m}$	= mass flux, g/cm^2
P	= pressure, atm
$\dot{q}$	= heat flux, W/cm^2
R	= radius, cm
$\dot{s}$	= recession rate, cm/s
T	= temperature, K
t	= time, s
α	= absorptivity
ε	= emissivity or emittance
ρ	= density, g/cm^3
σ	= Stefan-Boltzmann constant, W/m^2-K^4

Subscripts

c	= convective
cond	= conductive
cw	= cold wall
eff	= effective
f	= fail
g	= pyrolysis gas
n	= nose radius
r	= radiative
s	= stagnation point
t	= total
v	= virgin material
w	= wall
0	= without mass addition

Presented as Paper 93-2790 at the AIAA 28th Thermophysics Conference, Orlando, FL, July 6–9, 1993; received July 20, 1993; revision received April 15, 1994; accepted for publication April 15, 1994.

*Materials Engineer, Thermal Protection Materials Branch. Member AIAA.
†Chief, Thermal Protection Materials Branch.
‡Research Assistant.

Introduction

THE quest for future planetary missions has renewed interest in the development of high-temperature ablative heat shields. Space vehicles such as Mars and lunar-mission return vehicles will be entering Earth's atmosphere at velocities above 12 km/s and will experience severe heat loads.[1] Under this hypervelocity flight condition, the thermal protection system (TPS) will experience very high convective and radiative heat fluxes such that the use of an ablative heat shield becomes necessary. Recent studies show that low-density reusable surface insulation (RSI) such as Lockheed Insulation-2200 (LI-2200) may be used as ablative heat shields for some missions.[2] Numerical analysis and experimental data show that LI-2200 has a very low recession rate, mass loss with minimal melt runoff at low stagnation pressures, and moderate to high heat fluxes. However, at high pressure, LI-2200 suffered severe mechanical failure and spallation due to high shear load on the surface.

In an effort to improve upon the ablation characteristics and thermal performance of RSI, a unique family of new heat shields is being developed at NASA Ames called lightweight ceramic ablators (LCAs). These combine the benefits of both conventional ablators and low-density RSI. For example, one of the reasons that the conventional ablators performed well in a high-heating environment is their different heat dissipation mechanisms.[3] These mechanisms consist of 1) the energy absorption for depolymerization and gas pyrolysis of the organic resin, 2) heat blockage from the thickened boundary layer, and 3) the reradiation of the high-emissivity char layer. The low-density RSI, on the other hand, has very low conductivity and large void fraction and thus is a good insulator while retaining good specific strength.[4] The combination of the excellent high-temperature-capability of the ceramic substrate, due to its good insulative properties and high specific strength, with a high-blowing and/or charring infiltrant gives LCAs the capability to

Table 1 Composition and physical properties of LCAs

LCA I.D	Substrate composition, wt %	Substrate density, g/cm^3	Infiltrant	LCA density, g/cm^3
AI-8	98.5% SiO_2 1.5% SiC	0.126–0.141	None	0.126–0.141
AI-8-m	98.5% SiO_2 1.5% SiC	0.126–0.141	Pmma	0.215–0.233
s-LCA-m	LI-900 100% SiO_2	0.141–0.149	Pmma	0.213–0.237
s-LCA-p	LI-900 100% SiO_2	0.141–0.149	Phenolic	0.213–0.237
c-LCA	FMI 100% carbon	0.173–0.181	None	0.173–0.181
c-LCA-m	FMI 100% carbon	0.173–0.181	Pmma	0.224–0.248
c-LCA-p	FMI 100% carbon	0.173–0.181	Phenolic	0.224–0.248
c/Oak-LCA	Oakridge CBCF	0.272	None	0.272

provide protection against very severe thermal environments with substantial lighter weight than traditional ablators.

This paper will describe only the development and thermal responses of the low-density LCAs. The history of the LCA's development and characterizations are fully described in Ref. 5.

Materials

Lightweight ceramic ablators use porous ceramic and/or carbon fibrous substrates with densities of 0.0965–0.357 g/cm^3. Polymethyl methacrylate (pmma), phenolic, and water were used as infiltrants. Different impregnation techniques and curing procedures were developed for each infiltrant except water. LCAs have been produced with densities ranging from ≈0.224 to 0.256 g/cm^3 and are produced as follows. An organic infiltrant is first diluted with a solvent, and then the substrate is immersed in the solution. The solvent is then removed during a drying cycle to leave a desired amount of resin infiltrant. The LCAs are then slowly cured using two processes to insure a uniform distribution of the resin within the fibrous matrix. With this procedure, the fibers in the ceramic matrix are, in effect, coated with a thin film of resin. The final product has very low density with retention of large open-porosity volume fraction, good specific strength, and good insulation properties.

Table 1 shows the composition and physical properties of substrates and resins used in the development of LCA. The model identification of LCAs can be explained as follows. The first lowercase letter (or "AI-8") indicates the type of substrates, e.g., "s" stands for silica fibrous substrate, "c" for carbon, and "AI-8" for silica/silicon carbide (SiC). The last lowercase letter shown in the "LCA I.D." column represents the infiltrant. For example, "m" stands for pmma, "p" for phenolic, and "w" for water. If no infiltrant was used, then the substrate description stands alone, as with the c-LCAs.

The silica-based LCAs (s-LCAs) use fibrous silica substrates such as Lockheed Insulation-900 (LI-900). Another silica substrate used in the development of LCA is Ames Insulation-8(AI-8) which consists of 98.5% microquartz fibers and 1.5 wt % of SiC powder (21-μm-diam particle size). The addition of SiC particles will increase the AI-8's total hemispherical emittance and thus take advantage of reradiation as an additional means of rejecting heat at the surface.

The carbon-based LCAs (c-LCAs) used a carbon fiberform insulation manufactured by Fiber Materials, Inc. (FMI). The insulation is made of carbon fibers 14–16 μm in diameter and 1600 μm in length that are bonded by phenolic resin. Fiberform is a low-density, rigid, carbon-bonded insulation[6] that can be used in a vacuum or inert environment at temperatures up to 3,023 K. The insulation density varies from 0.128–0.200 g/cm^3. Another carbon material used was carbon-bonded carbon fiber (CBCF) material manufactured by Oak Ridge National Laboratory (identified in Table 1 as c/Oak-LCA). CBCF, developed for a radioisotope heat source, is made of small-diameter (10.5 μm) continuous rayon filaments that are precision chopped to 0.25 nm in length.[7] The fibers are carbonized at 1623 K and bonded with phenolic resin. The phenolic resin in the FMI insulation was completely pyrolyzed to bond the carbon fibers, whereas the phenolic resin in the CBCF was partially pyrolyzed and remained as particles within the fiber matrix.

Table 2 shows the composition and density of conventional ablators, and the test conditions under which each sample was evaluated. Avcoat 5026-39HC and SLA-561 were developed and used as ablative heat shields for the Apollo and Viking,[8] respectively. Both materials were used as benchmarks in the evaluation of the LCAs because they are flight-certified. The MA-25S, manufactured by Martin Marietta, is a medium-density ablator used as thermal protection on the external tank of the space shuttle. It is an elastomeric silicone-based material that can be applied by spraying or molding at room temperature.[9] Acusil-1, manufactured by Acurex Corporation, will be used as thermal protection on the COMET probe.[10]

Experiment

Facilities

Three test phases were conducted in two arc-jet facilities at Ames, the 20-MW Aerodynamic Heating Facility (AHF) and the 60-MW Interactive Heating Facility (IHF). An arc-jet facility is used to simulate heating conditions similar to those experienced by a space vehicle entering the atmosphere. The arc-jet facilities use a constricted arc heater to generate a high-temperature plasma stream. The test gas, which is air for the case of simulating earth re-entry, is heated by an electrical arc discharge confined with 6-cm-diam (AHF) or 8-cm-diam (IHF) constrictor column of the arc-heater.[11] After leaving the arc-heater column, the highly energized gas is supersonically expanded by a convergent-divergent nozzle and is discharged into an evacuated test chamber where the test model is located. The temperature, velocity, and pressure of the test gas can be varied by changing the nozzle area ratio (the area ratio of nozzle exit to nozzle throat). The available area ratios are 64–900 in the 20-MW AHF and 30–305 in the 60-MW IHF. The stream can attain enthalpies up to 45 MJ/kg and velocities up to Mach 8.

Instrumentation

The Instrumentation used in these tests was very simple. The model surface temperature was measured by a Thermogage pyrometer. A surface emittance of 0.9 was assumed for charring ablators and 0.50 for noncharring ablators.[12] In the 60-MW IHF, the heating rates and stagnation pressures were measured with a 1.588 cm-diam water-cooled copper calorimeter and pressure probe, whereas in the 20-MW AHF, the same measurement was made with a 5.08-cm-diam transient-type calorimeter. The sensing element for the latter calorimeter is a 0.793-cm-diam copper slug with a thermocouple embedded in the back. Three pressure orifices are spaced around the sensing element to measure the stagnation pressure. The calorimeters were used to determine the facility's power settings before ablation tests began. The test models and calorimeters were mounted on the facility to allow quick insertion at the center of the plasma stream in less than one second. Table 3 shows the nominal test conditions (i.e., cold-wall stagnation-point heat flux, stagnation pressure, exposure time, and model radius). The enthalpies listed in Table 3 were determined from the measured values of cold-wall convective heat flux and stagnation pressure by using the Fay-Riddell

Table 2 Test matrix for conventional ablators

Model I.D.	Composition	Density, g/cm^3	Test-condition heat fluxes, W/cm^2
Avcoat-5026-39HC	Phenolic microballoons, Novalac resin, phenolic honeycomb cells	0.5126	113 227 454 942
MA-25S (Martin Marietta)	Filled elastomeric silicone	0.400	113 227 454 942
SLA-561 (Martin Marietta)	Elastomeric silicone, silica fibers, carbon black, cork, microballoons,	0.288	942 1248
Acusil-1 (Aerotherm Corp.)	Silicone resin, flexcore glass phenolic H/C, quartz and phenolic microballoons, quartz fibers	0.481	113 227 454

equation,[13] assuming equilibrium nonfrozen flow, and the test gas was air in this case. We have

$$\dot{q}_{cw} = K\sqrt{\frac{P_{t2}}{R_n}}(h_t - h_w) \tag{1}$$

where $\dot{q}_{cw}$ is the cold-wall heat flux and $K = 1.124 \times 10^{-4}$.

In this case, h_w was neglected and assumed to be approximately equal to zero. This calculation also assumed that the calorimeter was fully catalytic.

Physical measurements and photographs were obtained both before and after the test, and surface recession rates were obtained from high-speed films.

The thermophysics of a noncharring ablative material can be illustrated by writing a general surface energy balance (SEB) equation

$$q_w = (1 - \alpha_{sw})q_r + F\sigma\varepsilon_w T_w^4 + q_{cond} + \dot{m}_{sw}(h_w - h_{sw}) \tag{2}$$

As described, the LCAs contain a rigid noncharring substrate with very high porosity and a pyrolyzing organic infiltrant. Heat dissipation mechanisms in the LCAs have different attributes from those in the general charring ablators because of the additional terms in the SEB. These attributes include in-depth energy, porosity, and thermal properties as functions of density, substrate melting, and mass decomposition. Milos and Rasky[14] summarized schemes to model the ablation characteristics of LCAs, and the SEB equation can be written as follows:

$$q_w = (1 - \alpha_{sw})q_r + F\sigma\varepsilon_{sw}T_w^4 + q_{cond} + (\dot{m}_{cw} + \dot{m}_{gw})h_w \tag{3}$$

$$q_{cond} = \dot{m}_{cw}h_{cw} + \dot{m}_{gw}h_{gw} + \dot{m}_{fw}h_{fw} - [\dot{m}_{cw} + \dot{m}_{gw} + \dot{m}_{fw}](h_s)_{\text{in depth}} \tag{4}$$

These relations take account of the thermochemical, kinetic limited, and fail (melting) models. In some instances, the most useful and least time-consuming engineering-level method in evaluating the materials' ablation characteristics and mass efficiency is to use the Q^* model. In this model, Q^* is the effective heat of ablation and is defined as follows[15]:

$$Q^* \equiv H_{eff} = \frac{-\dot{q}_{t0}}{\dot{m}} = \frac{\dot{q}_{c0} + \dot{q}_{r0}}{\dot{m}} \tag{5}$$

Here $\dot{q}_{t0}$ is the total heat flux without mass addition, and $\dot{m}$ is the mass loss rate. The negative sign designates heat received at the surface. The heating on a model's surface in the arc jet is mainly caused by convection. Thus the total heat flux $\dot{q}_{t0}$ is approximately equal to the convective term $\dot{q}_{c0}$, and

$$H_{eff} = \frac{\dot{q}_{c0}}{\dot{m}} \tag{6}$$

Table 3 Nominal test conditions

$\dot{q}_{cw}$, W/cm^2	Stag. pressure, atm	Enthalpy, MJ/kg	Nose radius, cm
113.5	0.014	13.60	2.54
227.0	0.0256	20.12	2.54
454.0	0.0609	26.09	2.54
942.0	0.081	33.19	1.27
1634.0	0.330	28.52	1.27

Because of the model configuration, the mass rate $\dot{m}$ used in the H_{eff} calculation is based on the stagnation recession rate $\dot{s}$ and the material's virgin density ρ_v:

$$H_{eff} = \frac{\dot{q}_{cw}}{\rho_v \dot{s}} \tag{7}$$

This relation allows for the nonuniformity of density among materials and uses only the recession at the stagnation point to give a meaningful presentation when comparing the thermal performance of different materials.

As shown in Fig. 1, all test models have a cylindrical configuration with a spherical nose. High-speed photography was used to record the ablation behavior of each model and to measure the recession rate $\dot{s}$. In addition, a 3.18-mm-spot-size optical pyrometer was used to measure the surface temperature of each sample during test.

Results and Discussion

Figure 1 compares the results obtained from arc-jet testing of c-LCA-p and the conventional ablator Avcoat. Posttest photographs were obtained of c-LCA-p and Avcoat samples tested at a cold-wall heat flux of 454 W/cm^2 for 60s. The density, recession, mass loss, and effective heat of ablation of each sample are listed in Fig. 1. As shown in the photograph, there is no significant change in shape or melting observed in the c-LCA-p sample. As shown by the black portion of the sample, pyrolysis of the phenolic resin took place only where the model was exposed to the plasma stream. The lighter-colored portion represents the virgin material that was protected by the model holder. Because of the limited availability of Avcoat material, a block of high-strength RSI (the white portion in the photograph) was used to mount the sample in the holder. The black portion of the sample is the charred Avcoat material. By contrast, a significant shape change (indicated by the bluntness on the model tip and melt runoff) was observed on the surface of the Avcoat sample. Most of the melt runoff was removed by the aerodynamic flow during the test. As shown in Fig. 1, the c-LCA-p sample has about one-third less recession and about 5 times higher effective heat ablation than the Avcoat sample. A review of high-speed film

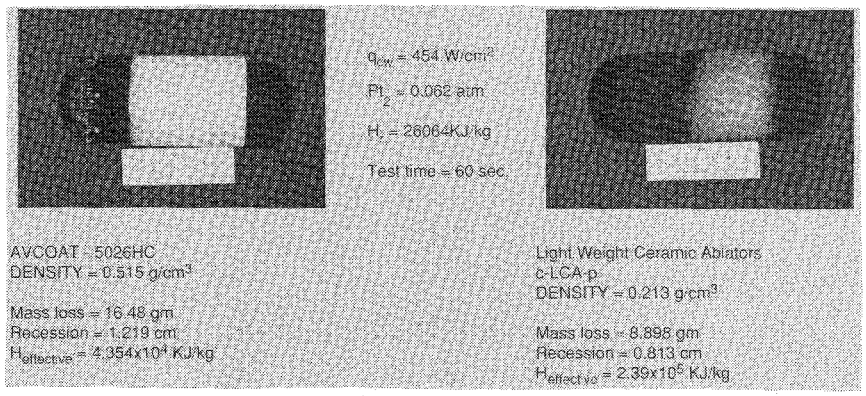

Fig. 1 Thermal performance of Avcoat 5026-39HC and c-LCA-p at $\dot{q} = 454$ W/cm^2 and $P_{t2} = 0.062$ atm.

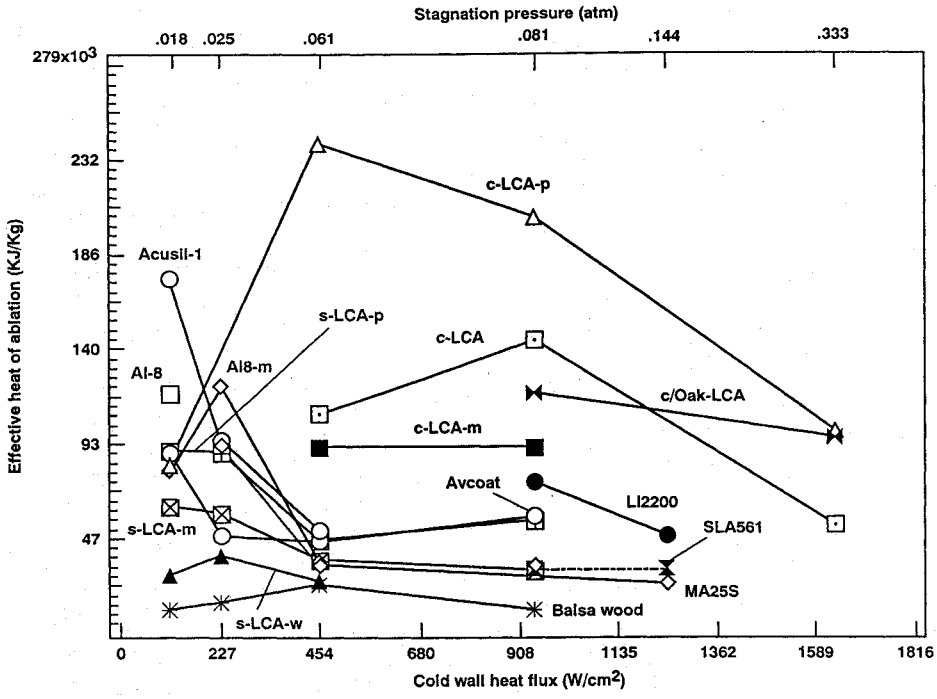

Fig. 2 Mass efficiency of lightweight ceramic ablators and conventional ablators.

data also indicates that spallation occured during the Avcoat test. This result shows a significant improvement in c-LCA-p thermal performance over the traditional ablators.

A complete summary of the mass efficiency of different materials tested in the arc jet is shown in Fig. 2. This figure shows H_{eff} plotted as a function of both cold-wall heat fluxes and stagnation pressures. The heat-flux levels were selected in an attempt to simulate the peak heating conditions of lunar (113.5–454 W/cm^2) and Mars mission (908–1634 W/cm^2) return trajectories. The stagnation pressure is the result of the facility adjustment to obtain the required heat fluxes. One general observation from Fig. 2, is that balsa wood, SLA-561, and s-LCA-w consistently have very low mass efficiency over a wide range of flux levels.

One notable feature in Fig. 2 is the predominant performance of the c-LCA at high flux levels (>454 W/cm^2), especially the very high efficiency of c-LCA-p. This can be attributed to the combination of several factors. First, the carbon substrate used in c-LCA has a very high melting temperature, so that an increase in surface temperature resulting from the formation of a char layer is not sufficient to cause the melting of the substrate. In addition, the carbon substrate has high surface emissivity ($\varepsilon \approx 0.9$), so that most of the energy absorbed at the surface is being reradiated. Another factor that contributes to the remarkable thermal performance of c-LCA-p may be the high charring characteristics of phenolic. This behavior is also illustrated by the low mass-loss fluxes of c-LCA-p at heat fluxes of 942 and 454 W/cm^2 shown in Figs. 3 and 4, respectively. Reradiation coupled with boundary-layer blockage is the most efficient mechanism in rejecting heat at the surface.[3] Surface reradiation seems to be the main mechanism for heat dissipation. Higher density at the surface resulting from the char deposition may be another contributor to the efficient performance of c-LCA-p.

Figure 2 also shows that the c/Oak-LCA is less efficient than the c-LCA and c-LCA-p at a heat flux of 942 W/cm^2. The difference in performance of the c/Oak-LCA and c-LCA-p may be due to several factors. First, phenolic in particle form might not be as efficient in rejecting heat as the phenolic film that resulted from the new infiltration technique. Second, c/Oak-LCA is made of smaller-diameter and shorter carbon fibers and thus may suffer microspallation at a lower temperature than c-LCA. Visual inspection reveals that the distribution of carbon fibers in the FMI insulation substrate is much more uniform than that of the CBCF materials.

At a heat flux of 942 W/cm^2, the ablative characteristics of LI-2200 seem to be consistent with those described by Henline et al.,[2] and the material has a lower recession rate and higher effective heat of ablation than that of the Avcoat-5026HC-39. One of the reasons for this behavior is that at low stagnation pressure the LI-2200 is more energy-absorbing and tends to reradiate the more energy without having high mass loss. Visual inspection of the posttest LI-2200 sample showed that there is a thin melt layer (approximately 1.5 μm) on the surface. The Avcoat material is less efficient, as shown from the result in Fig. 2, because of the gas pyrolysis of organic resins and melt runoff of the honeycomb structure.

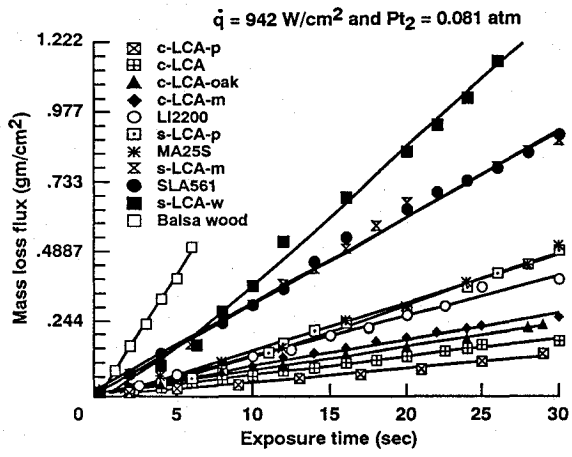

Fig. 3 Mass loss flux as a function of time.

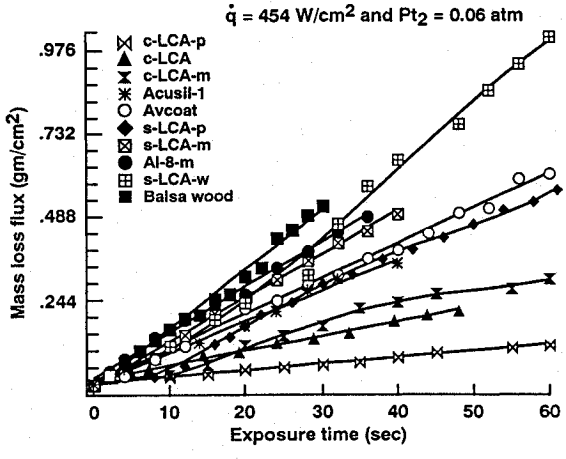

Fig. 4 Mass loss flux as a function of time.

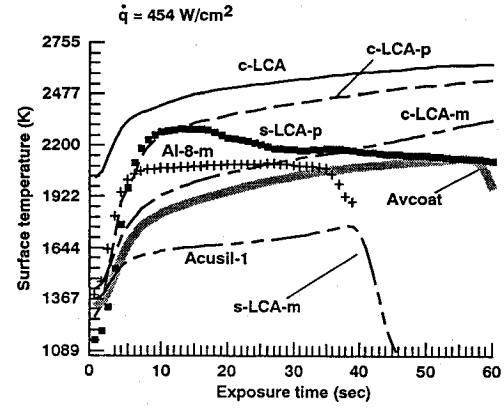

Fig. 5 Mass loss flux as a function of time.

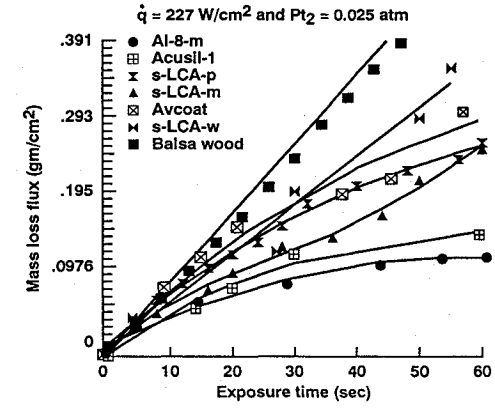

Fig. 6 Corrected surface temperature obtained from an optical pyrometer.

The transpiration cooling effect from the high gas pyrolysis rate of pmma did not improve the performance of c-LCA, because of the increased density. This would explain the decrease in mass efficiency of c-LCA-m observed in Fig. 2. Also note that the mass loss fluxes of c-LCA-m shown in Figs. 3 and 4 are consistently lower than those of the c-LCA and c-LCA-p.

Figure 4 also shows that s-LCA-p has an induction period (≈8 s) because of the initial gas pyrolysis of phenolic and char formation. Gas pyrolysis of phenolic has a much lower blowing rate, so that in rejecting heat at the surface the transpiration cooling mechanism becomes less efficient. However, the decomposition of the phenolic deposited a thick char layer on the surface, thus taking advantage of the reradiation mechanism, but at the same time causing an increase in surface temperature. This increase in temperature is sufficient to cause melting but not vaporization of silica substrate. Posttest analysis of the sectioned s-LCA-p sample showed a 0.525-cm-thick char layer beneath a few micrometer-thick silica melt layer.

Shown in Fig. 5 are the corrected surface temperature plots obtained from an optical pyrometer for the c-LCAs, s-LCAs, and selected conventional ablators at a heat flux of 454 W/cm^2. This figure illustrates the effect of the gas pyrolysis rate on the surface temperature of tested samples. The pmma in the c-LCA-m and the s-LCA-m samples acts as a transpiration coolant and results in a lower surface temperature (e.g., a difference of about 300 K between c-LCA and c-LCA-m, as shown in Fig. 5). The high charring characteristic of the phenolic shows a similar response in surface temperatures of the c-LCA-p and s-LCA-p samples. The surface temperature of the s-LCA-p was briefly increased and was correlated with the induction period observed in Fig. 4. The drop in the s-LCA-p temperature was caused by the sample receding past the focus point of the pyrometer. The rapid surface temperature decrease in the Acusil-1 indicates severe spallation, and the sample was removed at 40 s. The surface temperature of Acusil-1 is much lower than Avcoat and c-LCA because of the higher mass fraction of polymer in the reinforced honeycomb structure. Surface temperature of both AI-8-m and s-LCA-m are similar because of the presence of pmma and are comparable to Avcoat.

Figure 2 also shows that at the lowest flux level, the Acusil-1 and AI-8 outperform the conventional ablators and other LCAs. The addition of SiC in the silica substrate increases the total hemispherical emittance[16] of AI-8 and thus significantly improves AI-8's performance. The addition of a high-blowing infiltrant such as pmma increases the density and reduces the mass efficiency of the AI-8. This suggests that, at this flux level, the most efficient way to reject energy is by reradiation rather than passive transpiration. Another interesting observation at this flux level is that the c-LCAs have lower effective heat of ablation because of the dominance of the kinetic mechanism—that is, the oxidation of carbon is more favorable.

At a flux level of 227 W/cm^2, the results in Fig. 2 suggest that the most efficient materials are those with 1) substrates that reradiate most of the absorbed energy, and 2) infiltrants that absorb the most energy during gas pyrolysis. The efficiency of Acusil-1 and Avcoat decreases drastically, but the efficiency of s-LCA remained unchanged. In contrast to the results at lower flux levels, the addition of the high-blowing characteristics of pmma to AI-8 significantly improves mass efficiency. This can be seen by the lowest mass-loss flux of AI-8-m shown in Fig. 6. It occurs because AI-8-m contains both high-emittance AI-8 substrate and the high-blowing-rate pmma infiltrant.

In the case of s-LCA-m, the high gas pyrolysis rate was not sufficient to keep the surface cooled, and a large amount of energy was conducted toward the substrate, causing the silica to melt [larger q_{cond} term in Eq. (3)]. A significant amount of melt runoff was observed on the surface of the s-LCA-m sample, and some of the melt was blown away by the aerodynamic force of the gas stream. A 0.317-cm-thick layer of char beneath a thick coalescent melt layer was observed in the sectioned sample. The char layer was formed by the molecular cracking of the hydrocarbons—a decomposition product of pmma. The results from Fig. 6, along with visual observation,

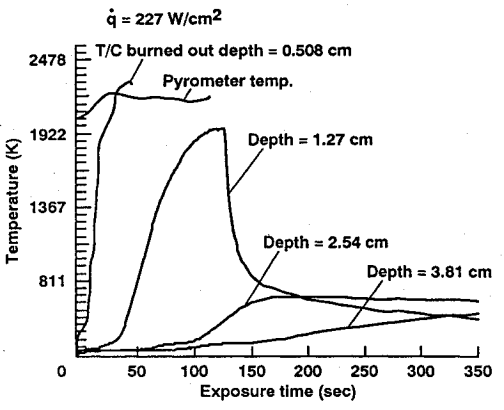

Fig. 7a Temperature profile of s-LCA-p.

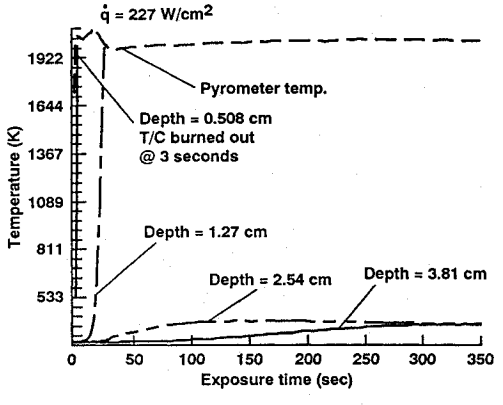

Fig. 7b Temperature profile of s-LCA-m.

confirm that the combination of high blowing rate of the infiltrant and high surface emittance of the substrate is the reason for the high mass efficiency of the AI-8-system.

Finally, Figs. 7a and 7b illustrate the effect of char forming on the surface and in-depth temperatures obtained from test samples instrumented with thermocouples. Several observations can be made from these plots. First, the temperature of s-LCA-p at 0.508-cm depth is slightly higher than that of the s-LCA-m. The reason for this small difference in T_s is the formation of a char layer beneath the melt layer of the s-LCA-m's surface. Second, as expected, the in-depth temperatures of the s-LCA-m are much lower than those of the s-LCA-p because of the higher thermal conductivity of the phenolic resin. The thermocouple data were also used as another means to obtain the recession rates.

Conclusions

Experimental data indicate that high-temperature, high-specific-strength structural ceramic ablators can be developed by using a correct combination of fibrous substrates and organic infiltrants. To date, LCAs have been successfully produced with various ceramic insulators such as silica, silica-alumina, and carbon fibers, and different-char-yield organic resins. Experiments were conducted to evaluate the thermal performance and ablation characteristics of the LCAs and to compare their performance with that of traditional ablators. At heat fluxes below 227 W/cm^2, the presence of pmma and SiC in silica substrates (AI-8) significantly reduced the mass loss and recession rates. The AI-8, Acusil-1, and AI-8-m are the most efficient systems, whereas the basal wood and s-LCA-w are the least efficient. The mass efficiency of s-LCAs, especially s-LCA-p, remains unchanged and is superior to that of Avcoat and MA-25S. At flux levels above 454 W/cm^2, the c-LCAs outperformed the s-LCAs and conventional ablators by a substantial margin. Test results also indicated that c-LCA-p has the highest effective heat of ablation and the highest potential for ablative-heat-shield application for planetary mission vehicles. Thermochemical ablation analysis and detailed characterizations are needed to further evaluate the thermal responses of AI-8, s-LCA-p, and c-LCA.

References

[1]Tauber, M. E., and Sutton, K., "Stagnation-Point Radiative Heating Relations for Earth and Mars Entries," *Journal of Spacecraft and Rockets*, Vol. 28, No. 1, 1991, pp. 40–42.

[2]Henline, W. D., Tran, H. K., and Hamm, M. K., "Phenomenological and Experimental Study of the Thermal Response of Low Density Silica Ablators to High Enthalpy Plasma Flow," AIAA Paper 91-1324, June 1991.

[3]Banas, R. P., Dolton, T. A., Housten, S. J., and Wilson, R. G., "Lifting Entry Vehicle Thermal Protection Review," Lockheed Co. Report 4-83-4-2, 1964.

[4]Leiser, D. B., Smith, M., and Stewart, D. A., "Options for Improving Rigidized Ceramic Heat-Shields," *Ceramic Engineering and Science Proceedings*, Vol. 6, Nos. 7–8, 1985, pp. 757–763.

[5]Tran, H. K., "Development of Light-Weight Ceramic Ablators," NASA TM-108798, Dec. 1993.

[6]Reynolds, C. D., and Ardary, Z. L., "Low-Density Carbon Fiber Composites," Y/DA-6925, Oak Ridge National Lab., Oak Ridge, TN, 1976.

[7]Wei, G. C., and Robins, J. M., "Carbon-Bonded Carbon Fiber Insulation for Radioisotope Space Power Systems," *American Society Bulletin*, Vol. 64, No. 5, 1985, pp. 691–699.

[8]Bartlett, E. P., and Andersen, L. W., "An Evaluation of Ablation Mechanisms for the Apollo Heat Shield Material," Aerotherm Report No. 68-38, Part II, Oct. 1968.

[9]Williams, S. D., and Curry, D. M., Thermal Protection Materials Thermophysical Property Data, NASA RP-1289, Dec. 1992.

[10]Beck, R. A. S., and Blaub, B., "Materials Development for Multiple Performance Requirements," Society of Automotive Engineers, Rept. 840920, July 1984.

[11]Balter-Peterson, A., Nichols, F., Mifsud, B., and Love, W., "Arc Jet Testing in NASA Ames Research Center Thermophysics Facilities," AIAA Paper 92-5041, Dec. 1992.

[12]Henline, W. D., "Aerothermodynamic Heating Environment and Thermal Protection Materials Comparison for Manned Mars-Earth Return Vehicles," AIAA Paper 91-0697, Jan. 1991.

[13]Fay, J. A., and Riddle, F. R., "Theory of Stagnation Point Heat Transfer in Dissociated Air," *Journal of Aeronautical Science*, Vol. 25, No. 2, 1958.

[14]Milos, F. S., and Rasky, D. J., "Numerical Procedures for Three-Dimensional Computational Surface Thermochemistry," AIAA Paper 92-2944, July 1992.

[15]Howe, J. T., "Hypervelocity Atmospheric Flight: Real Gas Flows Fields," NASA RP-1249, Nov. 1990, pp. 151–153.

[16]Goldstein, H., Leiser, D. B., Smith, M., and Stewart, D. A., "Opacified Silica Reusable Surface Insulation (RSI) for Thermal Protection of the Space Shuttle Orbiter," 15th International Thermal Conductivity Conference, Ottawa, Canada, Aug. 1977.